Climate Dynamics (2002) 18: 563–578
DOI 10.1007/s00382-001-0199-3

A. M. Waple · M. E. Mann · R. S. Bradley

# Long-term patterns of solar irradiance forcing in model experiments and proxy based surface temperature reconstructions

Received: 31 August 1999 / Accepted: 14 August 2001 / Published online: 5 February 2002


**Abstract** Comparisons are made of long-term empirical and model-estimated patterns of solar irradiance forcing during a 200-year period (1650-1850), which precedes any apparent anthropogenic influence on climate. This interval encompasses a considerable range (approximately 4 $W/m^2$) of estimated variation in solar output, including the "Maunder" and "Dalton" Minima of solar irradiance, and an intervening interval of relatively high values of irradiance, but does not encroach into the industrial era wherein it is difficult to separate solar and anthropogenic influences. Particular emphasis is placed on comparing empirical and modeled patterns of forced surface temperature variation. The empirical patterns bear a greater similarity to the pattern of forced response of a coupled ocean-atmosphere general circulation model (AOGCM) than with an independent model simulation result using an ocean with specified heat transport, both in terms of the spatial pattern of response and implied global mean sensitivity to forcing. Heightened sensitivity in the western Pacific warm pool apparent in the empirical response pattern, is not observed in the forced response of the coupled model. It is possible that this pattern is the result of feedback processes not currently reproduced in course-resolution coupled models. The greatest empirical response is found at the multidecadal-to-century ( > 40 year period) time scale, for which the forcing is dominated by the roughly 90-year Gleissberg Cycle of irradiance. This indicates a global-mean sensitivity (approximately 0.3 $K/W/m^2$), which is close to the coupled model result (approximately 0.4 $K/W/m^2$). At decadal time scales (8-25 year period), for which the forcing is dominated by the 11-year and 22-year period solar cycles), the temperature sensitivity is moderately reduced, and its spatial pattern of response is dominated by an apparent resonance with known decadal modes of climate variability.

A. M. Waple (✉)
National Climatic Data Center, 151 Patton Ave,
Asheville, NC, 28801, USA
E-mail: anne.waple@noaa.gov

R. S. Bradley
Department of Geosciences,
Morrill Science Center,
University of Massachusetts,
Amherst, MA, 01003, USA

M. E. Mann
Department of Environmental Sciences,
Clark Hall, University of Virginia,
Charlottesville, VA, 22903, USA

## 1 Introduction

As the central issue in climate change research shifts from the detection and attribution of anthropogenic climate change, to the estimation of its past, current, and likely future impact, it becomes increasingly important to reduce uncertainty in estimates of the response of the climate system to enhanced radiative forcing. Such a goal is potentially best accomplished by deducing more robustly, the relationship between radiative forcing of climate, including not just anthropogenic forcing but key natural radiative forcings such as solar irradiance changes, and the response or "sensitivity" of the climate to those forcings. Such efforts can elucidate the relative contributions of natural variability and human influence in observed climate change, helping to frame with realistic uncertainty estimates, forecasts of anthropogenic climate change.

Given a model-based prediction of the patterns of forced climate variability, and an estimate of the patterns and amplitude of natural climate variation, model-based "fingerprint" detection approaches (e.g., Houghton et al. 1995, Chap. 8; Marshall et al. 1995) provide one means of estimating the extent to which anthropogenic forcing has played a role in observed twentieth century climate trends. Such studies are limited, however, in that they rely upon the small amount of

information contained in the short twentieth century temperature record against which the model-predicted patterns are compared. The shortness of this record becomes problematic in the context of the possible role of natural climate forcing. Solar irradiance forcing, in particular, appears to exhibit most of its variability at multidecadal and longer time scales (e.g., Hoyt and Schatten 1993; Lean et al. 1995; Fröhlich and Lean 1998; Damon and Peristykh 1999), time scales just barely sampled by the instrumental record. The problem of detecting solar influence in twentieth century climate record is further hampered by the great similarity with greenhouse radiative forcing in both its (increasing) twentieth century temporal trend (see e.g., Lean et al. 1995), and its apparent surface spatial fingerprint (e.g., Marshall et al. 1994). For this reason, solar influences can only be confidently established by examining a period during which greenhouse radiative forcing played little role in governing climate variations, a condition which is very unlikely met for the period going back to at least the mid nineteenth century (e.g., Lean et al. 1995; Mann et al. 1998), the very period during which widespread instrumental temperature data are available.

Therein lies the particular value of proxy climate information (e.g., tree rings, corals, ice cores, varved sediments, and historical documents) which can be used to provide an empirical description of climate variations prior to the availability of widespread instrumental climate information (see Bradley and Jones 1993; Hughes and Diaz 1994; Lean et al. 1995; Mann et al. 1995a, 1998; Overpeck et al. 1997; Briffa et al. 1998; Jones et al. 1998). Recently, Mann et al. (1998, henceforth, "MBH98") produced reconstructions of global surface temperature patterns several centuries back in time, employing "multiproxy" networks of diverse high-resolution climate proxy data, calibrated and verified against the modern instrumental surface temperature record (see also Mann et al. 1999,2000a,b). Such reconstructions provide a reasonably detailed empirical picture of surface temperature changes over the globe for at least the past several centuries. Significantly, it is over precisely this time frame that we can best document the time histories of the most significant plausible forcings of climate (e.g., greenhouse gas, solar irradiance, and explosive volcanism) and are thus, well placed to diagnose long-term forced and unforced climate variability from an empirical perspective (see Lean et al. 1995; Crowley and Kim 1996; Overpeck et al. 1997; MBH98; Mann et al. 2000b; Crowley and Kim 1999; Damon and Peristykh 1999). It should be noted however, that both the reconstructions of solar irradiance and that of temperature further back than the instrumental measurements support, are by definition, estimates. There is much literature to suggest that the reconstructions we employ are reasonable and as reliable as possible (references appear throughout the text), but we make no claims that these reconstructions compare to measurements in their accuracy.

Where such long-term empirical studies, and model-based fingerprint detection studies of twentieth century climate change overlap, they share certain important conclusions. For example, MBH98, exploiting the distinct statistical attributes of solar and greenhouse-forcing trends on longer-than-century time scales, detected a significant influence of solar irradiance forcing on the early (but not late) twentieth century hemispheric warming (as well as significant warming following the Maunder Minimum of solar activity during the seventeenth century). This conclusion was subsequently confirmed, albeit with some level of uncertainty, in an independent model-based fingerprint detection study of twentieth century climate variability (Tett et al. 1999). Proxy based studies can estimate the long-term relationships that exist between the histories of climate forcing and response in the *actual* climate system, and gauge significance against *empirical* estimates of century-scale variability. By contrast, comparisons of modeled and observed twentieth century rely on the faithfulness of the model in capturing the myriad and complex features of the true climate system. On the other hand, only model-based studies can explicitly incorporate physical processes in the problem of signal detection. The two approaches are thus, in large part complimentary, and the most robust inferences result where these two approaches reach similar conclusions.

It is the intent of this study to directly compare both empirical and model-based diagnoses of the spatial and temporal patterns of solar irradiance forcing during a 200 year period (1650-1850) preceding any likely anthropogenic role in climate change. We focus not just on the global and hemispheric mean sensitivities to forcing, but examine in some detail the regional patterns of response and their timescale dependence, and in so doing gain insight into the possible underlying dynamical mechanisms associated with the response of the climate to solar forcing. In Sect. 2, we describe the empirical data (solar irradiance and surface temperature reconstructions) used in the study, as well as the model simulations to which we compare empirical results. In Sect. 3, we discuss the empirical and model-based patterns of apparent sensitivity of surface temperatures to solar irradiance forcing. In Sect. 4, we provide a summary and concluding comments.

## 2 Description of empirical data and climate models analyzed

The variation in irradiance, as measured over the last two decades by satellite-borne instruments is quite modest ($\sim$1-1.5 W/m$^2$ at the top-of-the-atmosphere between peaks and troughs in the solar cycle e.g., Willson 1997; Fröhlich and Lean 1998), fueling some uncertainty as to whether or not solar irradiance changes farther back in time are likely to have been sizeable enough to force significant climate variations. Since direct estimates of solar variability are not available prior to the 1970s, it is necessary to resort to indirect means of estimating solar irradiance variations. Records of mean monthly sunspot numbers are available from the early seventeenth century onwards as a proxy indicator of solar activity (earlier than this, cosmogenic isotopes trapped in ice cores can provide an alternative means of estimating changes in solar activity). Of

interest in this study are two independent reconstructions of solar irradiance, which calibrate this information in different ways, the reconstructions of Lean et al. (1995) and Hoyt and Schatten (1993). The Lean et al. (1995) (henceforth LBB95) reconstruction used in the empirical analyses described in the present study, and in the model experiments of Rind et al. (1999) discussed later, combines several indicators of the sun's inconstancy (such as amplitude of the 11 year, Schwabe, sunspot cycle and observations of other sun-like stars) to produce estimates of total solar irradiance back to 1610 (Fig. 3A). Rind et al. (1999) extend this series to 1500 by calibration with $^{10}$Be and $^{14}$C cosmogenic isotopic data. The solar reconstruction of Hoyt and Schatten (1993, henceforth 'HS93'), used in the alternative modeling study of Cubasch et al. (1997) also discussed later, uses the length (rather than the amplitude) of the solar-cycle as proxy of solar irradiance variation. The resulting reconstruction of solar irradiance is greater in overall amplitude than the LBB95 estimate by approximately 20%, and lags the LBB95 reconstruction by ~20 years (Crowley and Kim 1996). Doubts have been raised (Fröhlich and Lean 1998) regarding the reliability of Hoyt and Shatten's (1993) means of estimating solar irradiance, due both to the underlying assumptions regarding solar physics, and the observation that the HS93 solar irradiance overestimates the actual irradiance increase over the past decade recorded in calibrated satellite measurements (and may therefore falsely attribute too much of the recent warming to solar forcing in correlation-based studies). Our faith in the Lean et al. (1995) series in particular, is also based on striking similarities with independent estimates of solar activity from cosmogenic isotopes measured in ice cores (10Be and 14C) which should also reflect such variability for solid physical reasons (McHargue and Damon 1991). While the distinction between the two reconstructions is relatively unimportant in modeling studies, which seek to diagnose self-consistent relationships between forcing and response, it is quite important in empirical analyses which rely upon the fidelity of estimates of past solar variability to diagnose their impact on past climate.

There, we employ the proxy based global surface temperature pattern reconstructions of Mann et al. (1998; see also 1999a, 2000a,b). These reconstructions make use of a widely distributed network of seasonal or annual resolution proxy climate indicators (details provided in the supplementary information of Mann et al. 1998). The individual indicators have been calibrated against the twentieth century instrumental surface temperature-represented in a reduced state in terms of its empirical orthogonal functions (EOFs), leading to the solution of an inverse problem in which global surface temperature patterns are reconstructed back in time over the spatial domain dictated by the coverage of twentieth century instrumental record, based on the information in the proxy data network. The reconstructions are independently verified with the sparser instrumental surface temperature data available from 1854-1901 (and, in a few locations, with instrumental temperature records available more than two centuries back in time). The resolved spatial detail in the surface temperature reconstructions is dictated by the number of reconstructed surface temperature eigenvectors, which in turn is largely dictated by the coverage available from the proxy indicator network back in time. From 1820 to the present, based on the entire network of 112 indicators, 11 eigenvectors are skillfully resolved, back to 1760, 9 eigenvectors, back to 1700, 5 eigenvectors, and back to 1600, 4 eigenvectors (see Mann et al. 1998 for further details). Prior to 1450, by comparison, only 1 degree of freedom is resolved; just a single degree of freedom is adequate for estimating global or hemispheric mean temperatures (in fact, Mann et al. 1999 extend the estimate of Northern Hemisphere mean temperature back to AD 1000 with evidence of significant reconstructive skill), but not for reliable inferences into regional variability. Figure 1 shows the northern hemispheric mean temperature reconstruction including error bars back to AD1000. For the time period of interest here (1650 to 1850), however, the degree of spatial variance resolved in the instrumental record by the 4 to 11 eigenvectors retained in the reconstructions (20% to 40% respectively) implies that coarse regional details, appropriate for comparison with the relatively low-resolution model simulation results considered, are reasonably resolved.

We analyze results from the integrations of two distinct climate models. The first is a simulation of the GISS atmospheric GCM, model II (Hansen et al. 1983), for which the resolution has been kept deliberately coarse for computational efficiency, with 8°×10°horizontal resolution and nine vertical layers in the atmosphere, (including two levels in the stratosphere). The atmosphere is coupled to a mixed-layer 'q-flux' (specified heat transport) ocean, which allows heat diffusion through the base of the mixed layer, but which, of course, limits any inferences into possible ocean dynamical responses or feedbacks to radiative forcing. The estimated model equilibrium sensitivity to radiative forcing is ~1 °C/W/m$^2$, which is considered to be at the high end of an estimated sensitivity range (Houghton et al. 1995). Model year 1 is AD1500, which is approximately 100 years before the period of interest. This is done to minimize the impact of model spin-up effects on the output after 1600. When the model is started later, the magnitude of the cooling during the Maunder Minimum is smaller. The estimates of heat diffusion through the base of the mixed layer are also critical since if heat diffusion ceases, the cooling response to the reduction in irradiance in the Maunder Minimum is twice as large (Rind et al. 1999).

The second model analyzed is the MPI/Hamburg coupled ocean-atmosphere GCM (Maier-Reimer and Mikolajewicz 1992; DKRZ, modeling group, 1993). This coupled model is also fairly coarse in resolution (T21 truncation, giving an average resolution of about 5.5 degrees in latitude and longitude) with 19 levels in the atmosphere and 11 in the ocean. The equilibrium sensitivity to radiative forcing in this model is ~0.6 °C/W/m$^2$. A control run (integrated for 700 years) with fixed solar irradiance at 1365 W/m$^2$ showed that a drift correction needed to be applied to the model which artificially enhances the variability. It was therefore decided that two solar-forced model runs, using initial conditions 160 years apart in the control experiment, ought to be run to better isolate the solar signal from the increased noise (Cubasch et al. 1997). The solar-forced runs were begun in 1700 and integrated to 1992 using the solar irradiance estimates of HS93 scaled so that the average value of irradiance agreed with the fixed value of solar forcing for the control run.The model also employs a 20-year spin-up period to gradually reduce irradiance to 1700 value since, the irradiance at 1700 is lower than the 'average'.

We have focused only on the period after 1650 for which the most reliable empirical data, both solar irradiance and surface temperatures reconstructions, are available, and for which one or more of the model-simulation results are available for comparison. It is unfortunate that the different model experiments employ two different estimates of irradiance and we acknowledge that this makes direct comparison between the model outputs difficult. However, since the models are based on internally consistent relationships between forcing and response, this still enables us to compare between the models for the *sensitivity* of the climate to solar forcing.

## 3 Solar-forced patterns in model and observations

In MBH98 a significant relationship was established between the estimated Northern Hemisphere mean surface temperature variations and the LBB95 solar irradiance reconstruction during the past few centuries, including a significant relationship between solar irradiance increases and the warming of the early twentieth century, and a significant warming from the Maunder Minimum to post-Maunder minimum period. From the latter transition, MBH98 estimated an approximate increase of 0.4 °C in response to an approximate 4 W/m$^2$ increase in total solar irradiance, giving an approximate sensitivity of 0.4 °C/W/m$^2$ (taking into account the Earth's cross-sectional surface area), similar to the global-mean response cited by Cubasch et al. (1997).

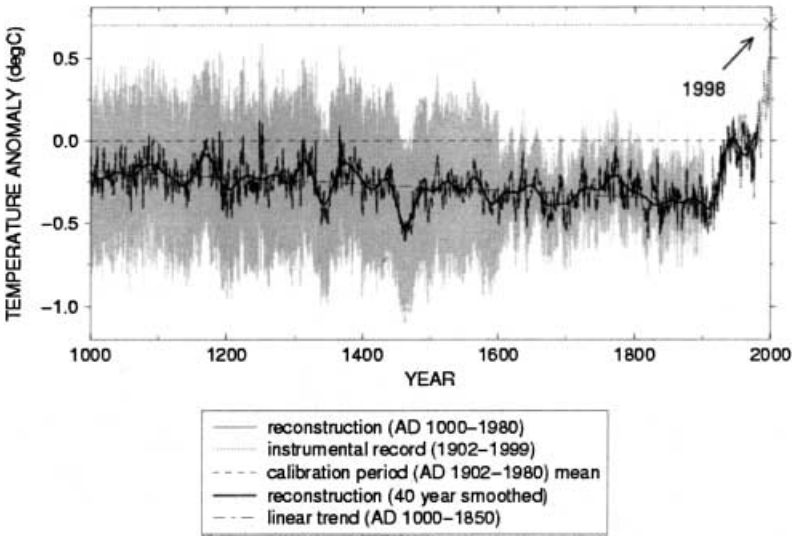


**Fig. 1.** Northern hemisphere temperature reconstruction of Mann et al. (1999) illustrating the two standard error limits (*shaded*)

Here we expand considerably on the MBH98 analysis, considering the patterns as well as hemispheric and global mean relationships between the empirical (LBB95) solar irradiance forcing and MBH98 temperature reconstructions, examining the time scale dependence of the spatial patterns of response and mean sensitivities, and explicitly comparing empirical and model-based results.

It is useful to use the more physically interpretable diagnostic of "sensitivity", rather than just correlation statistics, to guide our interpretation of solar-climate relationships. The sensitivity, $s$, as in Cubasch et al. (1997) can be estimated by linear regression,

$$s = \mathrm{cov}(T, F)/\mathrm{var}(F) \tag{1}$$

Where $T$ is the model or observed surface temperature (either global mean, or for a particular spatial region or gridpoint), $F$ is the forcing, and $s$ has units of °C/Wm$^2$. In the case of solar forcing, we take $F = S * 0.7/4$ where $S$ is the integrated total solar irradiance (e.g., the "Solar Constant"), while $F$ represents the associated average radiative forcing incident upon the Earth's surface, dividing by a factor of four accounting for the Earth's surface geometry and the half of the Earth not receiving sunlight, and multiplying by a factor of 0.7 accounts for the incoming shortwave radiation reflected back to space from the Earth's surface [assuming an albedo of 30%; note that Cubasch et al. (1997) employ a somewhat high value of 36% albedo in their calculations. We here use a more standard 30% albedo in all cases, including our assessment of the results of Cubasch et al. (1997) to provide a comparable sensitivity measure.

It is important to keep in mind that "sensitivity" defined in this fashion is an inherently linear concept, and becomes less applicable as non-linear dynamical feedbacks and processes become important. For the sake of our foregoing discussions, we will make the conventional assumption that the large-scale response of the climate system to radiative forcing can reasonably be approximated, at least to first order, by the behavior of the linearized system. It is also important to note that the sensitivity is based on correlation with global mean values of irradiance. It may be argued that a more appropriate correlation is one based on a latitudinally weighted value of irradiance. If this were to be approximated via an acknowledged weighting convention (i.e. something closer to $\Delta S \cos \phi(1\text{-}A/4)$, the correlation is however the same. This is due to the correlation being independent of the amplitude of the curves.

Equation (1), allowing for lag between $T$ and $F$ in the the covariance estimation is, in fact, a physically consistent means of estimated linear sensitivity to forcing under certain assumptions. It can be readily shown from energy balance considerations (White et al. 1998 provide an especially lucid treatment) that the linear response of a thermodynamically diffusive medium (e.g. either the ocean or the land surface, averaged over some appropriate depth) to an oscillatory variation in solar radiative forcing incident at the Earth's surface,

$$S = S_0 \cos(\omega t) \tag{2}$$

is simply,

$$T = T_0 \cos(\omega t - \phi) \tag{3}$$

where,

$$T_0 = S_0 \alpha (K^2 + \omega^2)^{-1/2} \tag{4}$$

with $\alpha$ depending only on properties (density, heat capacity, and skin depth) of the medium, and the delay,

$$\phi = \tan^{-1}(\omega/K) \tag{5}$$

depends only on the frequency of the forcing $\omega$ and the dissipation time scale $K^{-1}$.

In such a case, the sensitivity to the associated forcing,

$$s_S = T_0/S_0 \tag{6}$$

is correctly yielded by Eq. (1), where the covariance of $T$ and $S$ is evaluated at its maximum value with $T$ lagging $S$ by $\omega\Delta t = \phi$. While the sensitivity to an arbitrary solar forcing can be expressed in terms of an integral over frequency of the frequency-dependent response Eq. (4), it is instructive, as discussed later, to examine the frequency dependence of the sensitivity.

Under further approximation (assuming that the periodicity of the forcing is very long compared to the *dissipitation* time scale of the surface or near-surface response, and the forced variations in temperature are small compared to the global mean surface temperature of approximate 288 K), the Stefan-Boltzmann relationship can be used to yield the equilibrium (''blackbody'') approximation $s_S = 0.3$ K/W/m$^2$ for the sensitivity (see White et al. 1998). Because this represents an equilibrium response, it will overestimate the sensitivity if the time scale of the forcing is comparable to the dissipitation time scale of the system. It should also be kept in mind that the true sensitivity will be either greater than or less than this value if positive or negative dynamical feedbacks, respectively, are important at the global-mean scale of response. Cubasch et al. (1997) for example, using a coupled ocean-atmosphere model, estimate a global sensitivity $s_S = 0.4$ K/W/m$^2$, modestly greater than the blackbody response. Cane et al. (1997) argue that dynamical feedbacks involving tropical Pacific coupled ocean-atmosphere processes are not adequately represented in coarse-resolution coupled models, leading to a potential overestimation of the true sensitivity to radiative forcing in such models.

Alternatively, the low-frequency limit of (4) can be equated with the blackbody sensitivity, to yield an upper limit on the dissipitation time scale $K^{-1}$. This value can than be used in Eq. (4) to estimate the frequency dependent sensitivities semi-empirically, using estimated forcing amplitudes in different frequency bands. Applying the latter analysis to global (20°S-60°N) depth-averaged ocean temperature estimates during roughly the past 40 years, White et al. (1998) estimate a maximum dissipation time scale of $K^{-1} = 2.8$ years, implying sensitivity values $s_S = 0.22$ K/Wm$^2$ on interdecadal (15-30 year periods), and $s_S = 0.15$ K/W/m$^2$ on decadal (8-14 year) periods that are somewhat below the theoretical blackbody value ($s_S = 0.30$ K/W/m$^2$). Applying linear regression of estimated irradiance and the same ocean temperature estimates (e.g., application of ''1''), on the other hand, they calculate sensitivities very close to the blackbody value (see Table 1). Both methods yield estimates of lags of 0-2 years, on decadal and bidecadal time scales.

We favor here the purely empirical approach of Eq. (1) to estimating sensitivities, and subequently apply this approach to both proxy based surface temperature reconstructions and model simulation results. However, several caveats are essential to keep in mind in applying Eq. (1) to the estimation of sensitivity. Particularly, in the case of the empirical analysis, the regression estimates are more likely to provide a lower-bound approximation. Such caveats are discussed in more detail in the Appendix.

In Sect. 3.1 we examine the estimated patterns of sensitivity in both observations and two different forced model forced experiments, across timescales, or, for the ''integrated spectrum'' of the forcing. In Sect. 3.2 we focus on the multidecadal-to-century scale band of variability (longer than 40 year period) which contains the dominant component of the estimated solar irradiance variations (i.e., the roughly 90 year period Gleissberg cycle, and in Sect. 3.3, we focus on the decadal band (9-25 year period) which captures the higher-frequency (11 and 22 year cyclic components) of solar variability.

## 3.1 Integrated spectrum of forcing

### *3.1.1 Correlations and significance*

We first established the significance of the domain-averaged (global mean) relationship between the empirical MBH98 temperature estimates and the LBB95 solar irradiance series during the 1650-1850 period. It should be noted that 'global mean' in the Mann et al. series is dominated by the Northern Hemisphere due to the sparseness of data in the Southern Hemisphere. The lack of grid squares containing data at the highest northern and southern latitudes is however, not as problematic, since areal weighting affords them less importance as contributors to global or hemispheric means. Where there is a large discrepancy between Northern and Southern Hemisphere, it is noted in Table 1. This only occurs in one circumstance. The correlation between the global mean temperature series and the LBB95 series over this interval is 0.26 at lag 0 which is significant at the 99% level based on a one-sided test, taking serial correlation into account. The value increases to a maximum of 0.35 at a lag of 14. For comparison, MBH98 estimated a correlation $r = 0.4$ between the Mann et al. (1998) Northern Hemisphere mean temperature series and the LBB95 solar irradiance series over the same interval, significant at the 99% level. This correlation was found to increase very modestly (by 0.03) to a maximum with temperatures lagging irradiance by 10 years (Mann et al. 2000b).

We subsequently estimated the pattern of significant response by correlating each grid point in a map of the reconstructed surface temperatures with the LBB95 solar irradiance reconstruction during the same (1650-1850) interval of time. Significance must in this case be established by a two-sided test since, unlike hemispheric or global mean temperatures for which a positive response can be required based on *a priori* physical considerations, the sign of the response spatially can in fact take on both negative and positive values (see e.g., Cubasch et al. 1997; White et al. 1998). Even with this more conservative criterion, the resulting correlation map exhibits broad coherent spatial regions of significant response, as shown in Fig. 2 at zero lag, as well as at 14 year lag corresponding to the maximum correla-

**Table 1.** Empirical and model-based estimates of global mean sensitivity to solar irradiance forcing for both integrated spectrum of forcing, and invividual frequency bands. Indicated are (top) peak sensitivity over all possible delay or "lag" with respect to forcing and (bottom) value of delay (in years) at which maximum response is achieved

| | Integrated | >40 year | 9–25 year | 8–15 year | 15–30 year |
|---|---|---|---|---|---|
| Maximum sensitivity in degrees C/W/m$^2$ | | | | | |
| WMB01 | 0.24 | 0.25 | 0.17[b] | | |
| | nh 0.25 | nh 0.26 | nh 0.19 | | |
| | sh 0.22 | sh 0.24 | sh 0.13 | | |
| CUB97 | 0.39 | 0.41 | 0.21 | | |
| RLH99 | 1.13 | 1.10 | 0.36 | | |
| WCL98 | | | 0.19[a] | 0.15 | 0.22 |
| WCL98$^2$ | | | 0.28[a] | 0.27 | 0.29 |
| BBDY | 0.30 | | | | |
| MBH00b | 0.40 | | | | |
| Lag corresponding to maximum sensitivity (in years) | | | | | |
| WMB01 | 10–14 | 15 | 1.5+/–1.5 | | |
| CUB97 | 1 | 1–2 | 6 | | |
| RLH99 | 10–15 | 0–15 | 3 | | |
| WCL98 | | | 2.2[a] | 2 | 2.4 |
| WCL98$^2$ | | | 0.5+/–2.5[a] | 0+/–2 | 1+/–3 |
| BBDY | 0 | | | | |
| MBH00b | 10 | | | | |

WMB01 Waple et al. (current analysis 2001) empirical proxy-based surface temparature analyses
CUB97 Cubasch et al. (1997) ECHAM coupled ocean-atmosphere model experiment
RLH99 Rind et al. (1999) GISS atmospheric model w/specified ocean heat flux
WCL98$^1$ White et al. (1998) modern semiempirical [inverse energy balance calculation]
WCL98$^2$ White et al. (1998) modern empirical [linear regression of observations]
MBH98 Mann et al. (1998) – estimate of peak/trough Maunder Minimum change
MBH00b Mann et al. (1999) – estimate of lag for maximum solar-temperature correlation
BBDY Blackbody equilibrium estimate
[a]Approximated by the average of estimates in the 8–15 and 15–30 year bands
[b]Greater discrepancy between Northern and Southern Hemisphere means

tion with global mean temperatures. The patterns emphasize substantial positive correlations with continental interiors and large portions of the tropics, and low correlation (and even significant negative correlation) over substantial regions of the extratropical oceans. The potential significance of such regional variations is discussed later. Having established broad areas of significant apparent response of surface temperatures to solar forcing, we now focus, instead on the more easily interpreted diagnostic of "sensitivity", as discussed earlier.

### *3.1.2 Global mean sensitivity*

Empirical and model-estimated global mean sensitivities were estimated from linear regression (i.e., application of Eq. 1) of the Mann et al. (1998) empirical temperature reconstructions and the Rind et al. (1999) GISS model temperatures against the LBB95 solar irradiance reconstruction, and the Cubasch et al. (1997) MPI coupled model results against the HS93 solar irradiance reconstruction, each as a function of lag. It is worth noting that this quantity can be calculated either through an areally weighted sum over the individual gridpoint sensitivities, or, based on the global mean temperature series alone, owing to the linearity of the regression (Eq. 1) with respect to temperature. The global-mean sensitivities for both model and proxy-based observations (including the "integrated spectrum" and distinct multidecadal/century scale and decadal bands, see subsequent sections) are summarized in tabular form (Table 1).

The estimated global mean sensitivity at lag 0 is $s = 0.17$ °C/W/m$^2$ for the empirical analysis, $s = 0.36$ °C/W/m$^2$ for the MPI coupled model, and $s = 1.06$ °C/W/m$^2$ for the GISS model. In the case of the empirical analysis, the global-mean sensitivites take on their maximum value at a 14-year lag, the GISS model at a 10-year lag and the MPI coupled model's maximum global mean sensitivity is at a lag of one year (see Table 1) relative to forcing, with a value $s = 0.24$ °C/W/m$^2$ for the empirical sensitivity, $s = 0.39$ °C/W/m$^2$ for the MPI coupled model, and $s = 1.13$ °C/W/m$^2$ for the GISS model. The empirical estimate is remarkably similar to the empirical estimates of White et al. (1998) which are based on an entirely different (depth-averaged rather than surface temperature) dataset and a distinct, modern inverval of time. It should nonetheless be kept in mind that the latter estimates are based on only decadal time scale relationships, rather than the long-term variations implicit in the former. We might thus (e.g., through Eq. 4) expect less attenuation, and a modestly higher sensitivity at the longer multidecadal and century timescales. In fact, given the tendency of the empirical approach to underestimate sensitivity from the application of Eq. (1) due to the uncertainty in the actual forcing history (see discussion in Appendix 1), our empirical sensitivity should not be

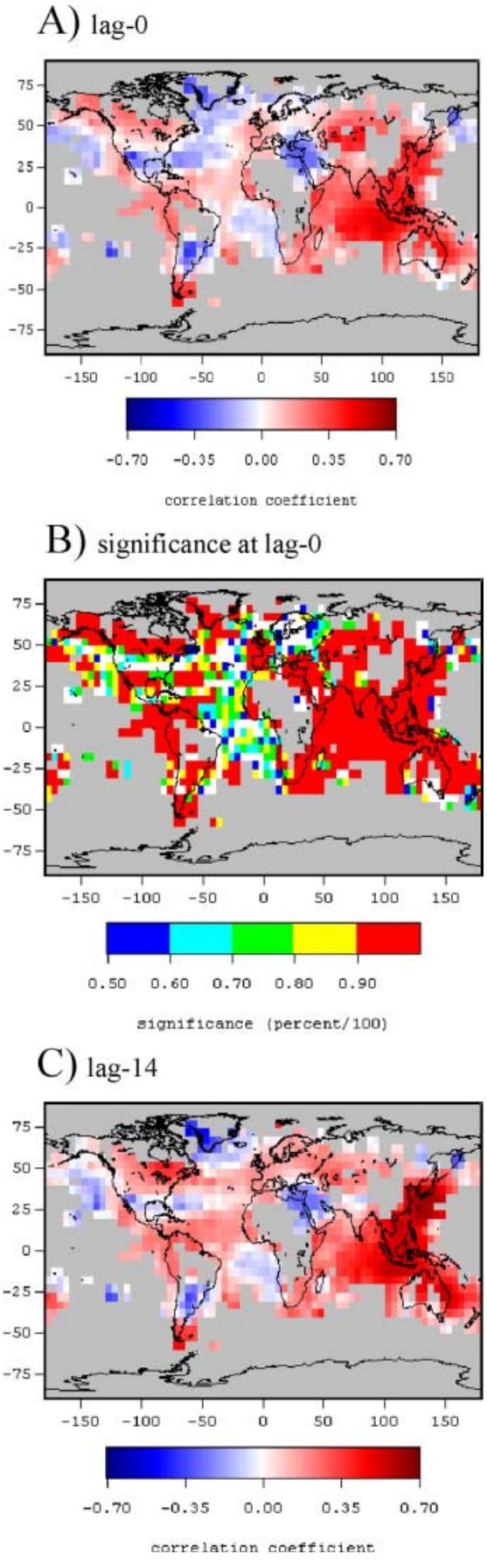


**Fig. 2A–C.** Correlation pattern between Mann et al. (1998) proxy-reconstructed surface temperature patterns and Lean et al. (1995) solar irradiance reconstruction for the period 1650-1850. Significance levels are shown at the 50-60% level (*dark blue*), 60-70% level (*cyan*), 70-80% in *green*, 80-90% in *yellow* and and >90% (*red*) based on a two-sided test taking into account serial correlation. Shown are both correlation patterns for lag = 0 and correlation pattern for lag = 14 corresponding to maximum global-mean correlation. Missing data is masked with a *gray background*

considered inconsistent with the slightly higher value (0.4 °C/W/m$^2$) found in both the MPI coupled model experiment, and cited by Mann et al. (1998) based on the observed mean temperature change from the period encompassing the Maunder Minimum (late 1600s) to the late 1700s (a moderate solar maximum). This GISS model, however, exhibits a sensitivity that is substantially greater than any of the other model or empirical estimates. This is discussed in more detail later. Figure 3 compares the empirical and two model global mean temperature variations during the 1650-1850 interval.

### *3.1.3 Spatial patterns of sensitivity*

The spatial patterns of sensitivity provide greater insight into potentially important regional dynamics and feedbacks. Notable in the empirical sensitivity pattern (Fig. 4A) are the large regions of positive sensitivity in the extratropical continental interiors, and very small or even sizeable negative sensitivities in the North Atlantic and northern North Pacific (giving rise to a strong land-ocean contrast to the sensitivity pattern), as well as greater sensitivity in the tropical versus extratropical oceanic regions. These features are remarkably mirrored in the solar "fingerprint" provided by the MPI coupled model experiment (Figure 4B).The similarities are even more evident when the pattern of the low-frequency component of the response is isolated, and the time-evolving patterns of low-frequency response are examined (see Sect. 3.2). Negative sensitivites in the subtropical South Atlantic found in the empirical pattern are not observed in the MPI model pattern.

Significantly, the relatively enhanced positive sensitivity in the western tropical Pacific 'Warm Pool' (relative to the eastern and central Tropical Pacific) observed in the empirical pattern is not evident in the MPI model pattern. This latter feature *may* be associated with a feedback mechanism outlined by Cane et al. (1997) and Clement et al. (1996).These studies suggest that the imposition of a uniform external positive radiative forcing should reinforce the negative temperature gradient across the Pacific basin through the Bjerknes feedbacks; since the source of cool upwelled waters in the Eastern Pacific suppresses any initial warming, the negative temperature gradient is initially enhanced. Once this enhanced gradient is established across the Pacific, an increase in trade wind strength exacerbates the gradient by enhanced upwelling in the east and a further increase in thermocline slope. Thus, according to these studies,

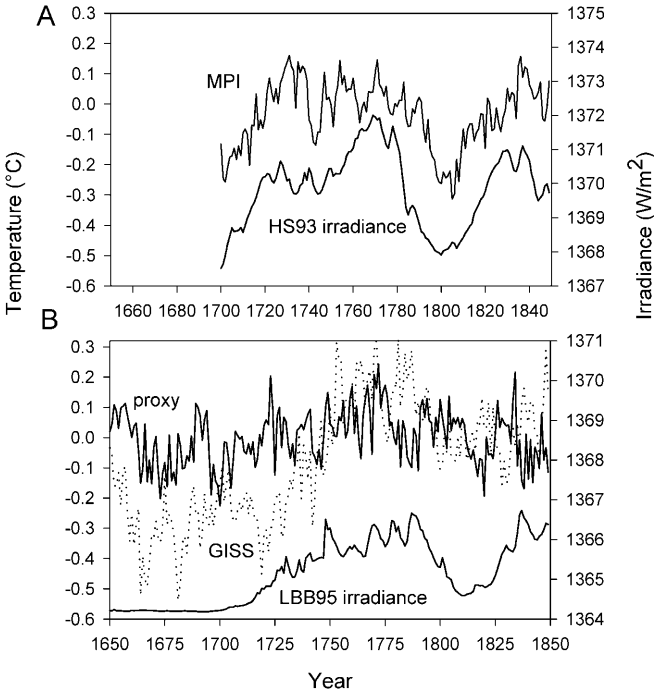


**Fig. 3.** Temperature versus solar irradiance time series. **A** Global mean temperature output of from the MPI model integration (average over the two independent integrations performed by Cubasch et al. 1997) and Hoyt and Shatten (1993) irradiance reconstruction, with which the model was forced. **B** Proxy reconstructed global mean surface temperature (*solid line*) (Mann et al. 1998), GISS simulated global mean temperature (*dotted line*) (Rind et al. 1999) shown along with the Lean et al. (1995) irradiance reconstruction used in the GISS model simulation to calculate the empirical forcing relationships

we might expect the western Pacific to exhibit enhanced positive sensitivity to solar radiative forcing relative to the eastern tropical Pacific. Cane et al. (1997) suggest that such a feedback is not adequately represented in most coupled ocean-atmosphere models due to a dynamic coupling between the equatorial ocean and atmosphere which is too weak in such coarse resolution models, and thus presumably absent in both of the model simulations we have analyzed here. It is at least a plausible explanation for the observed discrepancy between the models and the empirical pattern. Further analysis is required before we can suggest this consis-

►

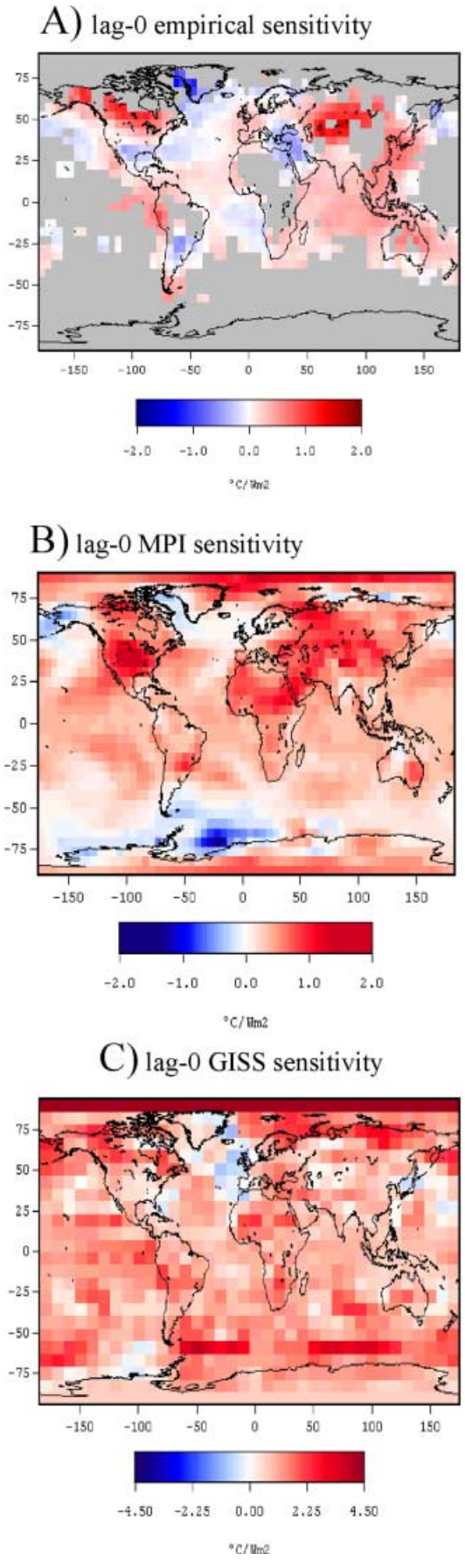


**Fig. 4.** Maps of sensitivity of surface temperature with respect to solar irradiance forcing for the integrated spectrum of solar irradiance forcing at zero lag. **A** Empirical sensitivity pattern of Mann et al. (1998) surface temperature reconstructions against the Lean et al. (1995) solar irradiance series for the period 1650-1850. **B** MPI simulated temperature sensitivity (Cubasch et al. 1997) relative to the Hoyt and Schatten (1993) irradiance reconstruction over the period of 1700-1992. **C** GISS simulated temperature sensitivity relative to the Lean et al. (1995) solar irradiance reconstruction, over the same period (1650-1850) as in **A**. As in similar following plots, regions without data are masked by a *gray background*, and the amplitude of the sensitivity is indicated by the *color-scale provided*

tency with the Cane et al. (1997) argument is based on observable physical processes. It is also worth noting that this enhanced tropical sensitivity is found in a region which does not, in longer paleoclimate records (Holocene, Quaternary and Cenozoic), exhibit a great deal of sensitivity to external forcing. It is possible in this case that there are biases in the Mann et al. (1998) reconstruction. However, It is *also* possible, that the more recent past exhibits more variability in this region through such processes as ENSO, and that the boundary conditions of the last several hundred years allow a greater sensitivity than those prior to the last millennium. This apparent feature of the empirical sensitivity pattern at the very least, highlights the potential importance of tropical Pacific ocean-atmosphere dynamics in the climate response to radiative forcing, even if the true nature of that response is not readily yet agreed upon (e.g., Meehl and Washington 1996; Cane et al. 1997).

In contrast to the MPI model, the GISS model pattern (Fig. 4C) shows very little regional distinction in the exhibited spatial pattern of sensitivity, but rather displays ubiquitous positive sensitivity, except for a small area of the northern North Atlantic. The GISS model also exhibits very little evidence of any significant evolution in the pattern of response over time. The lack of a dynamical ocean in this case (see discussion in Sect. 3.2) is almost certainly a limitation to any favorable comparison with observed patterns of response.

Explicit comparisons of regionally averaged surface temperature time series from the MBH98 reconstructions with the LBB95 solar irradiance reconstruction (Fig. 5) help to illustrate some important regional relationships, and emphasize the apparent enhancement of sensitivity at multidecadal and longer timescales (see Sect. 3.2). Shown are regional series of the western tropical Pacific (Fig. 5, dashed line) which, as discussed, exhibits a particularly large-amplitude apparent response to forcing, and of the tropical North Atlantic (Fig. 5, solid line) which exhibits a response to the forcing that may be related (see discussion in Sect. 3.2) to the resonance of solar forcing with an intrinsic multidecadal made of the Atlantic that has been discussed elsewhere (Folland et al. 1986; Delworth et al. 1993,1997; Kushnir 1994; Schlesinger and Ramankutty 1994; Mann and Park 1994, 1996; Mann et al. 1995a, 1998; Timmermann et al. 1998; Delworth and Mann 2000). The variations in this multidecadal mode of climate variability most strongly impacting the subtropical North Atlantic are well represented by the time series of one of the reconstructed eigenvectors (the 5$^{th}$ EOF) of the MBH98 reconstructions (also shown in Fig. 5, dotted line, for comparison) which can be thought of as representing one standing component of this evolving multidecadal signal (see Delworth and Mann 2000).

## 3.2 Low frequency (multidecadal-to-century scale) band

### *3.2.1 Global mean sensitivity*

An analagous set of calculations to those described in Sect. 3.1 were performed, instead focusing on sensitivity in the multidecadal/century scale period band (time scales > 40 years). We applied Eq. (1) using the 40-year lowpassed versions of the temperature reconstructions and LBB95 solar irradiance series (the lowpass filtering was performed with a Hamming weights filter, favoured for long relatively stationary time series, see Stearns and David 1988). The global-mean lowpassed-filtered series from the Mann et al. (1998) temperature reconstructions, MPI, and GISS simulations are shown in Fig. 6. As discussed earlier, the GISS model exhibits clearly higher amplitude variability in response to the specified low-frequency solar irradiance variations suggested by

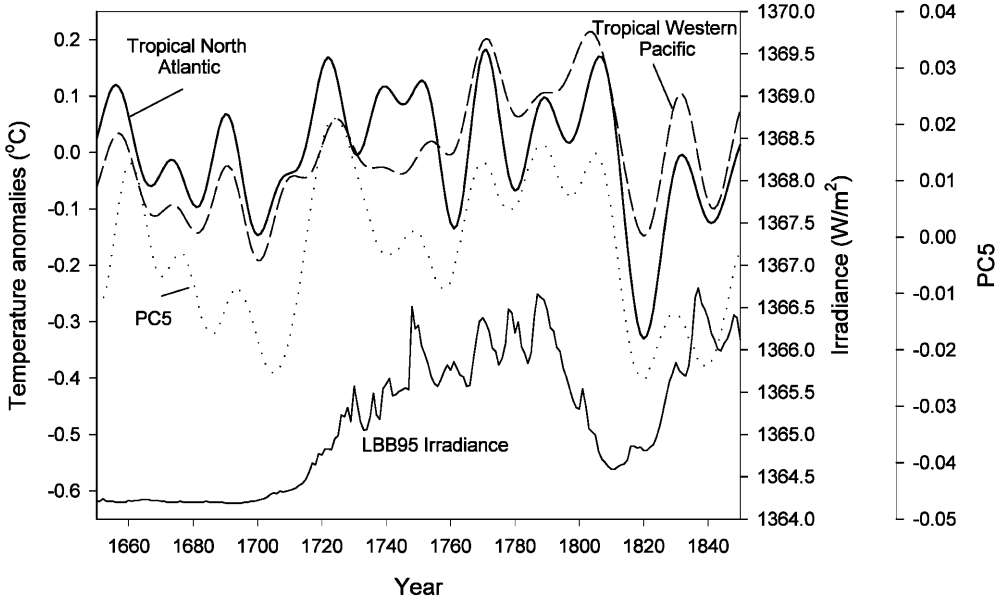


**Fig. 5.** Comparisons of time series of Mann et al. (1998) reconstructed regional temperature variations (15-year lowpassed data are shown) and Lean et al. (1995) solar irradiance series. Temperature averaged over a selected area of the tropical western Pacific (*dashed line*) (112.5°×137.5°lon by 22.5°N to12.5°S) and temperature average over a selected area of the tropical North Atlantic (*solid line*) (–67.5°×–27.5°lon by 22.5°N to 12.5°N). Also shown (*dotted line*) is the time-series of the 5$^{th}$ EOF identified in the Mann et al. (1998) study as representing the principal mode of multidecadal variability

either the empirical or MPI model. results. The GISS model's higher temperature variance can be attributed to the high equilibrium sensitivity of the model. The greater amplitude of the MPI model temperature variations relative to the empirical temperature estimates (see Fig. 6), is in large part related to the use of the HS93 solar irradiance series to force the MPI model, rather than the lower-amplitude LBB95 series (note e.g., Table 1, that the sensitivities, for example, are reasonably similar). Signal-to-noise considerations may explain the small discrepancies between the actual low-frequency sensitivities. For example, the average of an ensemble of two realizations used by Cubasch et al. (1997) should increase the expected signal-to-noise ratio by a factor of $2^{1/2}$, leading to smaller expected random departures from the true sensitivity in the estimates (see Appendix 1). More significantly, unlike the empirical estimates, the solar-only forced runs are not influenced by other external climate forcings. For example, MBH98 show that explosive volcanism leads to significant cooling during the early nineteenth century which is not accounted for in the solar-only forced model runs, but clearly plays a role in early nineteenth century evident in the low-passed empirical temperature series. In contrast, the solar-forced model temperatures increase during the early nineteenth century in response to solar-only forcing. Mean global sensitivites (see Table 1) in this low-frequency band are, for the empirical case, 0.21 at zero lag, reaching a maximum value at a 15-year lag (0.25), and declining thereafter. For the MPI model lag-0 sensitivity at this frequency is 0.40, reacing a maximum lag at 1-2 years (0.41), while the GISS model experiment shows a lag-0 sensitivity value of 1.10 which changes barely at all over 15 years of lag, but which is actually highest at lag-0.

### *3.2.2 Spatial patterns of sensitivity*

Figure 7 shows the empirical pattern of sensitivity at varying lag (0, 10, 20, 30) relative to forcing, spanning roughly one half period of the dominant time scale (about 90 years, i.e., the "Gleissberg Cycle") of low-frequency solar forcing. As these lower-frequency variations appear to dominate the global-mean sensitivities (see Table 1), it should not be considered surprising that the pattern at zero lag is, by-in-large, similar to that determined (Fig. 4) for the frequency integrated response. It is worth noting, however, that the low-frequency band, dominated by time scales that are large compared to the dissipation time scale of approximately three years (see earlier discussion), more effectively captures the equilibrium or near equilibrium response of the system. Indeed, the broad-scale features of enhanced land-sea contrast, and enhanced tropical SST response are more clearly captured (Fig. 7), while some of the more regionally-heterogeneous features (e.g., the tropical South Atlantic negative sensitivities) present in the integrated pattern of response, are far less evident in the low-frequency pattern of response. The former lower frequency features appear to be fundamental aspects of the equilibrium response to solar forcing (e.g., as in Cubasch et al. 1997), while these latter higher frequency features appear to be related to the resonance of solar forcing with the intrinsic decadal modes of the climate system (see e.g. White et al. 1998, and the detailed discussion of the higher-frequency patterns of response in Sect 3.4 see also Drijfhout et al. 1999 for further indications of solar forcing of internal climate variability).

Both the warming of the continental interiors and the enhancement of the tropical Pacific warm region become maximized, as does the global-mean sensitivity, between a lag of 10 and 20 years. After a lag of 20 years, the sensitivities in most regions of the globe begin to decrease. The evolving features of the North Atlantic are particularly interesting, as they appear to relate to a coupling of the forcing to internal multidecadal ocean-atmosphere variability centered in the basin. Especially notable are the appearance of negative anomalies in the North Atlantic through the evolution of the sensitivity pattern (see e.g.,

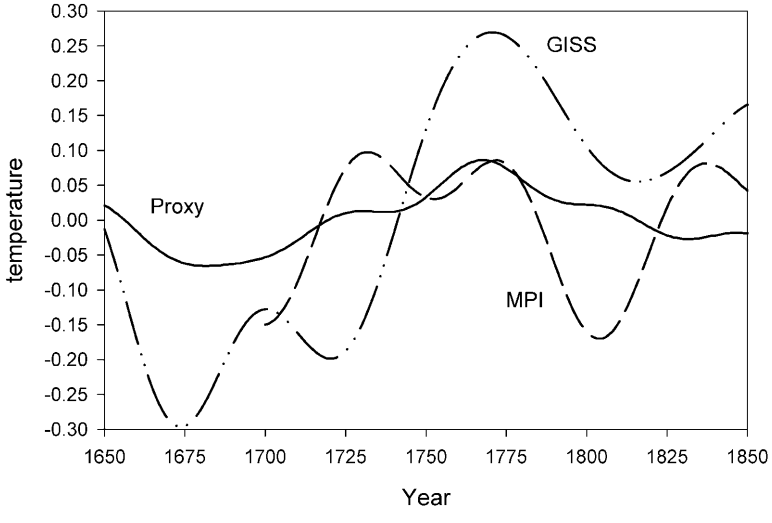


**Fig. 6.** The 40-year lowpassed filtered global mean temperatures of the proxy reconstructed temperature (Mann et al. 1998), the MPI simulated temperature (Cubasch et al. 1997), and the GISS simulated temperature (Rind et al. 1999). For the MPI temperature, an mean of the two runs was calculated, then filtered

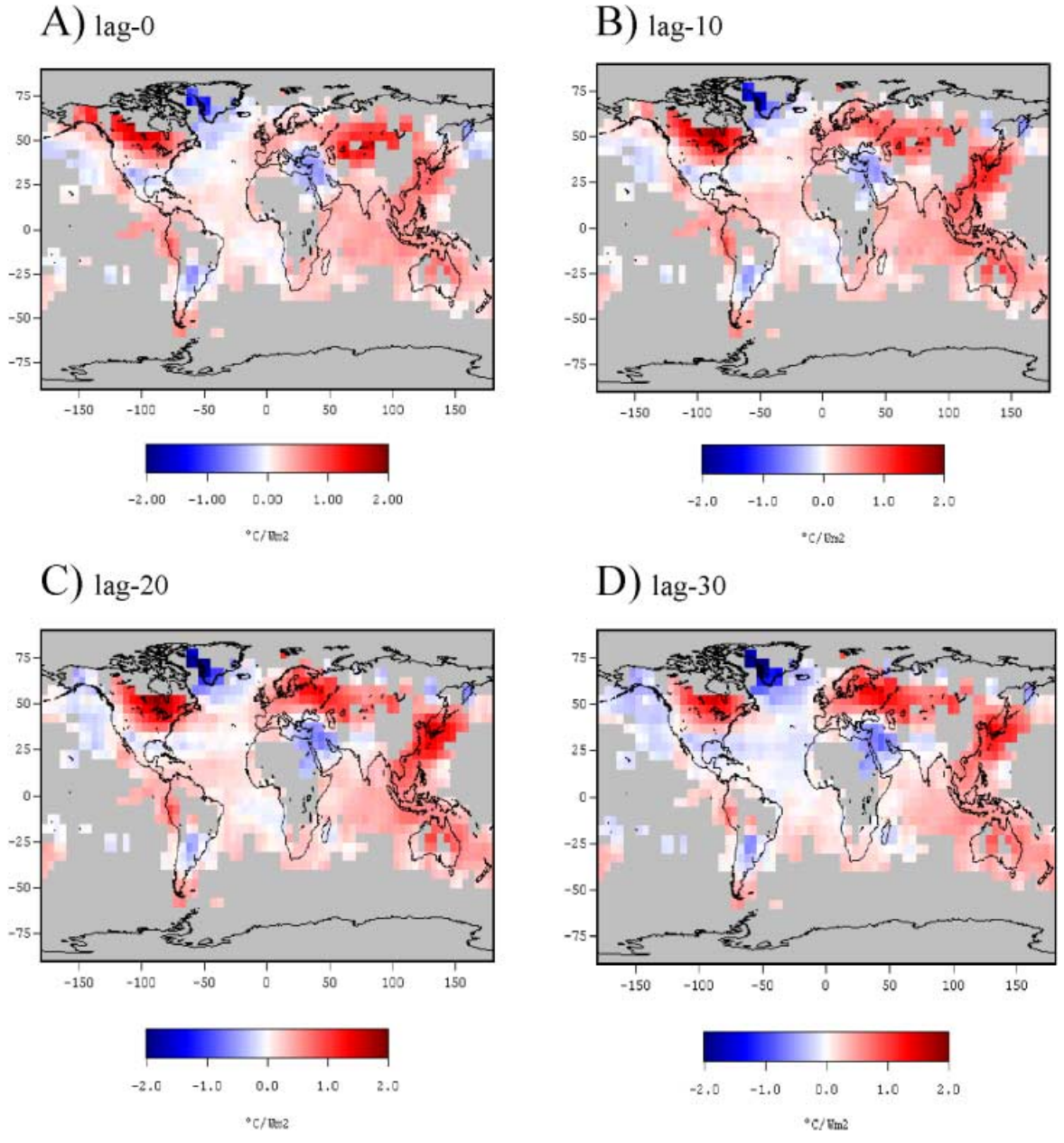


**Fig. 7.** Sensitivity of Mann et al. (1998) reconstructed temperature with respect to Lean et al. (1995) estimated solar irradiance in the multidecadal/century scale ( > 40 year period) band, at lags of **A** 0, **B**, 10 year, **C** 20 year **D** 30 year. The temperature and solar irradiance series were filtered using a Hamming weights lowpass filter with half-power cutoff centered at frequency 0.025 cycles/year

Fig. 7D), though negative sensitivities in the very northernmost parts of the region (i.e., near Greenland) remain throughout the evolution of the forced pattern.

Cubasch et al. (1997) attribute such negative sensitivites to solar forcing in the North Atlantic at lags of 25-30 years directly to an anticorrelation (–0.8) of the meridional overturning of the thermohaline circulation with irradiance. During the strongest change in irradiance in the HS93 reconstruction (between 1770 and 1830), the overturning of the THC was reduced by as much as 10% (Cubasch et al. 1997), leading to a decrease in the northward oceanic heat transport in the Atlantic, and a consequent cooling of temperatures. These changes are associated with a negative sensitivity (about –0.4) in the northern mid latitude temperatures that is maximum at a lag of 25 years in the MPI coupled model, and is closely mirrored in the empirical pattern at a lag of 30 years (Fig. 7D). This scenario is, in certain respects, similar to scenarios that have been suggested under conditions of greenhouse-induced warming (Manabe and Stouffer 1994; Stocker and Schmittner 1997). This same model (see Timmermann et al. 1998), as other models (e.g., the GFDL coupled model-see Delworth et al. 1993,1997; Delworth and Mann 2000) appear to exhibit variability in the North Atlantic thermohaline circulation at multidecadal time scales due to intrinsic

ocean-atmosphere processes, excited from stochastic forcing alone without the need of any external pacing.

The evolution in the North Atlantic exhibited by the empirical low-frequency sensitivity pattern to solar radiative suggests a scenario in which this intrinsic multidecadal mode of variability may indeed resonate with solar radiative forcing. The pattern at lag 30 years, closely resembles a particular phase (the reverse of the "120 degree" phase pattern shown in their Figs. 5 and 7) of both the empirical (as isolated in the MBH98 surface temperature pattern reconstructions) and modeled (as observed in long integrations of the GFDL low-resolution coupled ocean-atmosphere model) 60-70 year time scale signal discussed by Delworth and Mann (2000) (for comparison, this represents roughly 90 degrees in phase, or 15 years, subsequent to the peak warmth in the subtropical North Atlantic as shown in Fig. 5). In the model, this phase of the signal is indeed associated with a minimum in the THC index. These observations thus suggest a resonance scenario in which solar forcing may impose this favoured phase of the natural multidecadal pattern and, in doing so, phase-lock the near-term evolution of the signal, at least during those (e.g., late eighteenth century and early nineteenth century) during which the multidecadal solar variations are particularly pronounced. In the abscence of such high-amplitude forcing, we would exhibit the multidecadal pattern to nevertheless exhibit free oscillatory behavior (see Delworth et al. 1993,1997; Timmermann et al. 1998; Delworth and Mann 2000). Such a scenario is consistent with the apparent partial phase-locking of the solar variations and multidecadal Atlantic SST variations shown in Fig. 5 (bottom).

The somewhat weaker negative sensitivities in the North Pacific evident in both the empirical and MPI coupled model sensitivity pattern could also be associated with the dynamical mechanisms outlined by Timmerman et al. (1998). Using the MPI coupled model, they argue that there is a direct atmospheric teleconnection between multidecadal North Atlantic SST anomalies, arising from changes in the strength of the thermohaline circulation, and atmospheric circulation patterns influencing SSTs in the North Pacific. Delworth and Mann (2000) confirm a similar, though substantially weaker, teleconnection into the North Pacific in the GFDL model and argue (as in Mann et al. 1995a) for a significant Pacific expression of multidecadal variability over the past few centuries based on long-term proxy data and proxy reconstructed temperature patterns. The observational study of Minobe (1997) confirms the existence of such multidecadal oscillatory behavior in the Pacific region and western North America. Some of the enhanced warmth in Europe and the United States, and cold anomalies in Greenland and in the Middle East, appearing to peak at 30 year lag in Fig. 5, are consistent with the observation of multidecadal/century-scale variations in the NAO (see e.g., Appenzeller et al. 1998), that appear to be tied, at least in part, to the multidecadal North Atlantic signal discussed already (Delworth and Mann 2000).

### 3.3 High-frequency (decadal) band

#### *3.3.1 Global-mean sensitivity*

In order to isolate the surface temperature sensitivity to solar irradiance forcing at decadal time scales, the temperature and irradiance were bandpassed in the 9-25 year period range (using, as in Sect. 3.2 a Hamming weights filter), and the sensitivity estimated through Eq. (1). The moderately lower sensitivites in the decadal band ($s = 0.18$), are consistent with an attenuated response relative to the lower-frequency sensitivities established in Sect. 3.2, expected from Eq. (4) since the time scale of forcing is in this case more comparable to the dissipitation time scale. The resulting sensitivity is quite close to that obtained by White et al. (1998) by their semi-empirical approach, averaged over a similar range of decadal-to-bidecadal time scales (see Table 1). The amplitude of the empirical sensitivity is nearly constant from lag 0 years (0.17) to lag 3 years (0.13) constraining the lag of the response to between 0 and 3 years (e.g., 1.5 +/–1.5 years), again consistent with the results of White et al. (1998).

#### *3.3.2 Spatial Patterns of sensitivity*

Figure 8 shows the empirical pattern of sensitivity at varying lag (0, 3, 6, 9, and 12 years) relative to forcing, spanning roughly one half period of the lower-frequency (22 year) time scale that dominates the 9-25 year period band. The pattern is far less dominated by the broad patterns evident at multidecadal time scales, which resemble the expected equilibrium patterns of response. Instead, more spatially heterogeneous patterns of negative and positive sensitivities are evident. At zero lag, for example, substantial negative sensitivites are evident over Europe, the southeastern USA/subtropical North Atlantic, and tropical South Atlantic (leading, in part, to the expression of simliar features in the integrated pattern of response shown in Fig. 4), while substantial positive sensitivities are observed in the tropical North Atlantic, tropical Pacific, and central Eurasia. The pattern of response is, in fact, characterized by strongly time-evolving features (compare panels A–E in Fig. 8) that are quite reminiscent of established decadal modes of the climate, including in the Atlantic region, the North Atlantic Oscillation (NAO) (Deser and Blackmon 1993; Hurrell and van Loon 1997) and tropical Atlantic Dipole (Tourre et al. 1999 and references therein) patterns dominated by quasidecadal time scales, and in the Pacific region, ENSO-like tropical and extratropical patterns (e.g., the Pacific North American or "PNA" pattern) of variability (see e.g., Trenberth 1990; Mann and Park 1993,1994,1996; Trenberth and Hurrell 1994; Graham 1994; Latif and Barnett 1994; Zhang et al. 1997; Miller et al. 1998; White and Cayan 1998) dominated by roughly bidecadal time scales. We point out to the reader that the decadal Atlantic variability in the

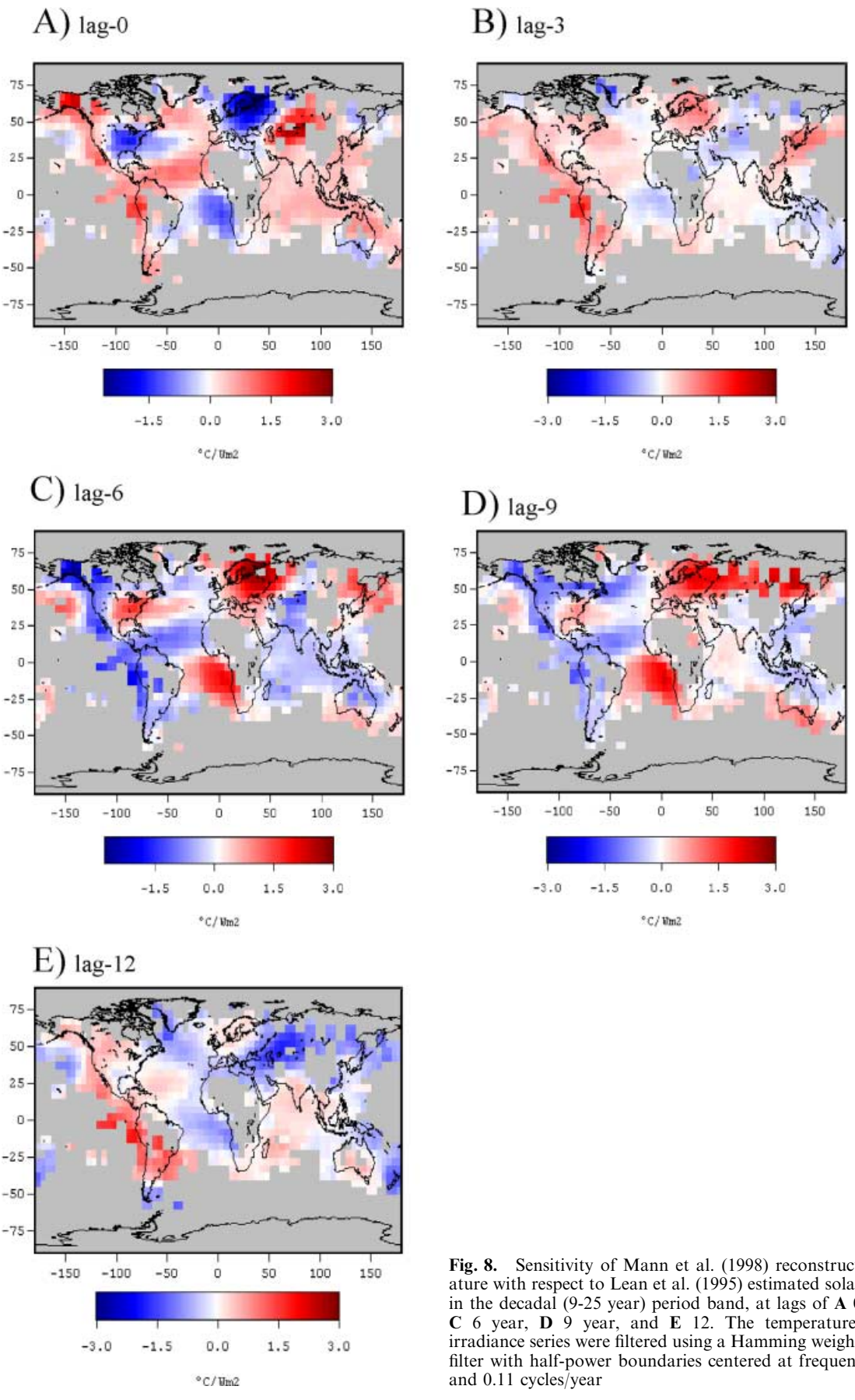


**Fig. 8.** Sensitivity of Mann et al. (1998) reconstructed temperature with respect to Lean et al. (1995) estimated solar irradiance in the decadal (9-25 year) period band, at lags of **A** 0, **B** 3 year, **C** 6 year, **D** 9 year, and **E** 12. The temperature and solar irradiance series were filtered using a Hamming weights bandpass filter with half-power boundaries centered at frequencies of 0.04 and 0.11 cycles/year

reconstructed temperature patterns are largely described by the pattern of the 3rd eigenvector (see MBH98), while the interdecadal ENSO-like variability in the MBH98 reconstructions are discussed in detail by Mann et al. (2000a). The finer decomposition into quasidecadal and bidecadal components of response is clearly of value, and we refer the reader to White et al. (1998) for such an analysis in the context of the modern climate record.

Quite analagous to the discussion in Sect. 3.2 of a possible resonance between low-frequency solar forcing and a natural multidecadal mode of the climate system, it would thus appear that the regional patterns of sensitivity to decadal time scale solar forcing (which often appear far more impressive than the modest global-mean response may in fact result from the resonance of the forcing with the internal decadal modes of the climate system. This observation has indeed been made with regard to the instrumental record. Mann et al. (1995b, see also Mann and Park 1996) find evidence that intrinsic large-scale quasidecadal patterns of climate variability appears to resonate with the 11 year solar cycle during periods of unusually high solar cycle amplitude (e.g., the past few decades), but not during periods of lower amplitude variability (e.g., the earlier decades of the millennium) during which the same mode may exhibit largely stochastically-excited internal variability. White et al. (1998) in fact observe a strong relationship between solar variability and the intrinsic decadal modes of the climate system during the past few decades. Cook et al. (1997) review, and demonstrate strengthened new dendroclimatic evidence, for a phase locking of 22 year time scale solar variations, and large-scale atmospheric patterns of continental drought in North America, during the past few centuries. Evidence thus appears to be mounting for the notion that decadal time scale solar forcing excites a response of the climate largely through such a resonance with internal modes of variability. It is possible, (see discussion in Mann and Park 1999) though far from certain, that this is caused by the stratospheric modulation of ozone concentrations (Haigh 1996) or cloud-electrification processes (Tinsley 1988) associated with solar variability. Significantly, however, such feedbacks do *not* appear to be significant at the global-scale since, as discussed, the spatial patterns of sensitivity average out to global-mean sensitivities in the 9-25 year band that appear to fall short of the (no-feedback) Blackbody estimates.

## 4 Discussion and summary

Empirical inferences into solar irradiance forcing are possible during an extended interval of time prior to widespread industrialization, 1650-1850, using indirect information to reconstruct both large-scale surface temperatures and solar irradiance forcing estimates. Comparisons of these empirical estimates of climate variability and forcing provide insights into solar influence on climate which, though not without their sources of uncertainty and limitations, are essentially immune from the typical contamination by anthropogenic influences. This latter feature makes such estimates an important independent check on any empirical inferences based on modern solar-climate relationships. Our empirical results lead to an estimate of global-mean sensitivity to solar radiative forcing very close to the Blackbody value (approximately 0.3 $K/W/m^2$), but certainly not inconsistent with the moderately higher values (approximately 0.4 $K/W/M^2$) of sensitivity estimated in the MPI coupled ocean-atmosphere solar-forcing experiment analyzed, taking into account the likelihood that the sensitivity is underestimated due to uncertainties in the empirical long-term solar forcing estimates.

Regional patterns of response in the observations, moreover, match in many respects, those isolated in the coupled model response to solar forcing, particularly with regard to the low-frequency variations. This includes the basic signatures of enhanced positive sensitivity in extratropical continental interiors, low/negative sensitivity in oceanic regions (together consituting a pattern of strong land-ocean contrast), and relatively enhanced SST sensitivity in the tropics. The complex and delayed empirical pattern of response of the North Atlantic to solar forcing appears to be mirrored in the coupled model response, resulting from a spinning-down of the thermohaline circulation (and consequent decrease in northward oceanic heat flux) in response to positive radiative forcing. There appears to be a relationship between this response, and possible resonance with an internal mode of variability in the North Atlantic that results from multidecadal time scale coupled ocean-atmosphere mechanisms. There is less similarity in both the mean estimates and spatial patterns of empirical sensitivity in the case of model experiments employing specified ocean heat transport, emphasizing the apparent importance of ocean dynamical processes in explaining observed patterns of sensitivity. In contrast to the low-frequency patterns, the pattern of response at decadal time scales appears to be dominated by a resonance of known modes of decadal climate variability with solar forcing, with relatively modest sensitivities at the global-mean scale.

Finally, there is some evidence in the empirical patterns of response of a dynamical feedback in the tropical Pacific which has been hypothesized as a potentially important negative feedback to positive radiative forcing (Cane et al. 1997), not captured in current generation coupled models. Accounting for the absence of such a feedback in the model could potentially bring both the global mean and pattern of the model sensitivities even more closely in line with the empirical estimates.

**Acknowledgements** We thank Judith Lean and David Rind and Rick Healy for providing solar irradiance estimates and results from the GISS model experiments, and we thank Reinhard Voss and Ulrich Cubasch for providing results from the MPI model simulations. Helpful suggestions from Tom Crowley are gratefully acknowledged, and we thank Frank Keimig for his technical assistance. This work was supported by the National Science Foundation and the Department of Energy. M.E.M. acknowledges

support through the Alexander Hollaender Distinguished Postdoctoral Research Fellowship program of the US Department of Energy. This work is a contribution to the NSF and NOAA-sponsored Analysis of Rapid and Recent Climatic Change (ARRCC).

## Appendix A

A note on the estimate of sensitivity from linear regression of forcing and temperature series

One can estimate *s*' (see e.g., Cubasch et al. 1997), the linear sensitivity with respect to a given forcing $F$ through linear regression,

$$s'_f = \langle FT \rangle / \langle F^2 \rangle \tag{7}$$

where $\langle FT \rangle$ is the covariance of $F$ and $T$, and $\langle F^2 \rangle$ is variance in the forcing series $F$. Since $T$ can be considered as a sum of the forced response to $F$ and a residual "noise term" $N$ (which actually consists of the response to other forcings as well as internal climate noise), we can write,

$$T = T_f + N \tag{8}$$

Allowing us to write the estimated sensitivity s' in terms of the true sensitivity s as,

$$s'_f = s_f(1 + \langle FN \rangle / \langle FT_f \rangle) \tag{9}$$

where

$$s_f = \langle FT_f \rangle / \langle F^2 \rangle \tag{10}$$

is the correct theoretical sensitivity. It is thus evident that the sensitivity as estimated through direct application of (Eq. 7) will in general differ from the true estimate of sensitivity (Eq. 10) for at least two distinct possible reasons:

1 *random errors:* sensitivity will differ from the true sensivity by some additive fraction (second term in Eq. 9) which depends on the signal-to-noise ratio through the ratio of the signal and noise covariances with the forcing for the given realization. This error term can be quite large in a relatively short single-realization, but in principle can be reduced if it is possible to average over an ensemble of more than one noise realization (e.g., Cubasch et al. 1997, –in an infinite ensemble, this term should of course average to zero) or over a very long interval of time. It is also possible to reduce the expected amplitude of this random error if the forcing and temperature series are filtered in bands where the signal-to-noise ratio for the forcing is greatest.

2 *systematic bias:* this is largely in issue only for empirically estimated sensitivities, which are based on statistically independent estimates of forcing and response, wherein calibration uncertainties and random errors can both lead to systematic errors in estimates of sensitivity (This is in contrast with the model-forcing experiments, wherein errors in the estimate of the actual forcing are immaterial, as it is only the self-consistent response of the model to any supplied forcing which is used to ascertain sensitivity). These systematic errors fall into two basic categories. The first will always lead to an underestimate of sensitivity, while the second can lead to either an underestimate or overestimate of sensitivity:

a Any random uncertainties in the estimate of the true history of the forcing will increase the variance of the forcing (the denominator in Eq. 7) but not (on average) the covariance of the forcing and temperature estimate (the numerator in Eq. 7), consequently leading to an underestimate of the true sensitivity.

b A systematic overestimate (underestimate) of variance in the calibration of the solar irradiance reconstruction will systematically decrease (increase) the sensitivity estimate, while a systematic overestimate (underestimate) of variance in the calibration of the temperature reconstructions will systematically increase (decrease) the sensitivity estimate.

Neglecting the calibration uncertainties (i.e., 'b') or at least being unable to determine *a priori* the likely sign of the associated bias in either case, we are left to conclude that the considerable uncertainty in the information used to extend solar estimates back in time insures substantial *random* uncertainty (i.e., 'a') in the forcing estimate, and necessitates that we consider the empirically estimated sensitivity patterns fundamentally as lower bound estimates of the true sensitivity. Because several of the possible sources of bias discussed above are likely to exhibit time scale dependence, examination of the sensitivity in independent frequency bands may however provide a means of establishing more confidence in the estimates. Estimates of sensitivity confined to frequency bands wherein the forcing history is most accurately estimated are less likely to lead to underestimates of sensitivity vis error source 'a'.

## References

Appenzeller C, Stocker TF, Anklin M (1998) North Atlantic oscillation dynamics recorded in Greenland ice cores. Science 282: 446–449

Bradley RS, Jones PD (1993) 'Little Ice Age' summer temperature variations: their nature and relavance to recent global warming trends. Holocene 3: 367–376

Briffa KR, Jones PD, Schweingruber FH, Osborn TJ (1998) Influence of volcanic eruptions on Northern Hemisphere summer temperature over the past 600 years. Nature 393: 350–354

Cane MA, Clement AC, Kaplan A, Kushnir Y, Pozdnyakov D, Seager R, Zebiak SE, Murtugudde R (1997) Twentieth-century sea surface temperature trends. Science 275: 957–960

Clement AC, Seager R, Cane MA, Zebiak SE (1996) An ocean dynamical thermostat. J Clim 9: 2190–2196

Cook E, Meko DM, Stockton CW (1997) A new asessment of possible solar and lunar forcing of the bidecadal drought rhythm in the western United States. J Clim 10: 1343–1356

Cubasch U, Voss R, Hegerl GC, Wazskewitz J, Crowley TJ (1997) Simulation of the influence of solar radiation variations on the global climate with an ocean-atmosphere general circulation model. Clim Dyn 13: 757–767

Crowley TJ, Kim K-Y (1996) Comparison of proxy records of climate change and solar forcing. Geophys Res Lett 23, 4: 359–362

Crowley TJ, Kim K-Y (1999) Modeling the temperature response to forced climate change over the last six centuries, Geophys Res Lett 26 13: 1901–1904

Damon PE, Peristykh AN (1999) Solar cycle length and 20th century northern hemisphere warming. Geophys Res Lett 26(16): 2469–2472

Delworth TL, Manabe S, Stouffer RJ (1993) Interdecadal variations of the thermohaline circulation in a coupled ocean-atmosphere model. J Clim 6: 1993–2011

Delworth TL, Manabe S, Stouffer RJ (1997) Multidecadal climate variability in the Greenland Sea and surrounding regions: a coupled model simulation. Geophys Res Lett 24: 257–260

Delworth TD, Mann ME (2000) Observed and simulated multidecadal variability in the North Atlantic. Clim Dyn 16, 661–676

Deser C, Blackmon M (1993) Surface climate variations over the North Atlantic ocean during Winter: 1990–1989. J Clim 6: 1743–1753

DKRZ model-user support group (1993) Report 6: the ECHAM3 general circulation model. Max-Planck Institute für Meteorologie, Hamburg, Germany

Drijfhout SS, Haarsma RJ, Opsteegh JD, Selten FM (1999) Solar-induced versus internal variability in a coupled climate model. Geophys Res Lett 26(2): 205–208

Folland CK, Palmer TN, Parker DE (1986) Sahel rainfall and worldwide sea temperatures. Nature 320: 602–606

Fröhlich C, Lean J (1998) The sun's total irradiance: cycles, trends and related climate change uncertainties since 1976. Geophys Res Lett 25(23): 4377–4380

Graham NE (1994) Decadal-scale climate variability in the 1970's and 1980's: Observations and model results. Clim Dyn 10: 135–162

Haigh J (1996) The impact of solar variability on climate, Science 272: 981–984

Hansen J, Russell G, Rind D, Stone P, Lacis A, Lebedeff S, Ruedy R, Travis L (1983) Efficient three-dimensional global models for climate studies: models I and II. Mon Weather Rev 111(4): 609–662

Houghton JT, Meira Filho LG, Callander BA, Harris N, Kattenberg A, Maskell K (eds) (1995) Climate change 1995: the science of climate change. Intergovernmental panel of climate change. Cambridge University Press, Cambridge, UK

Hoyt DV, Schatten KH (1993) A discussion of plausible solar irradiance variations, 1700–1992. J Geophys Res 98, A11: 18895–18906

Hughes MK, Diaz HF (1994) Was there a "Medieval Warm Period" and if so, where and when? Clim Change 26: 109–142

Hurrell JW, van Loon H (1997) Decadal variations in climate associated with the North Atlantic oscillation. Clim Change 36: 301–326

Jones PD, Briffa KR, Barnett TP, Tett SFB (1998) High-resolution palaeoclimatic records for the last millennium: interpretation, integration and comparison with general circulation model control run temperatures. The Holocene 8: 477–483

Kushnir Y (1994) Interdecadal variations in North Atlantic sea surface temperature and associated atmospheric conditions. J Clim 7: 141–157

Latif M, Barnett TP (1994) Causes of decadal climate variability over the North Pacific and North America. Science 266: 634–637

Lean J, Beer J, Bradley RS (1995) Reconstruction of solar irradiance since 1610: implications for climate change. Geophys Res Lett 22(23): 3195–3198

Maier-Reimer E, Mikolajewicz U (1992) Report 2: the Hamburg large-scale geostrophic ocean general circulation model, cycle 1. Max-Planck-Institute für Meteorologie, Hamburg, Germany

Manabe S, Stouffer RJ (1994) Multiple-century response of a coupled ocean-atmosphere model to an increase of carbon dioxide. J Clim 7: 5–23

Mann ME, Lall U, Saltzman B (1995b) Decadal-to-century scale climate variability: Insights into the Rise and Fall of the Great Salt Lake. Geophys Res Lett 22: 937–940

Mann ME, Park J (1993) Spatial correlations of interdecadal variation in global surface temperatures. Geophys Res Lett 20: 1055–1058

Mann ME, Park J (1994) Global scale modes of surface temperature variability on interannual to century time scales. J Geophys Res 99: 25819–25833

Mann ME, Park J (1996) Joint spatio-temporal modes of surface temperature and sea level pressure variability in the Northern Hemisphere during the last century. J Clim 9: 2137–2162

Mann ME, Park J (1999) Oscillatory spatiotemporal signal detection in climate studies: A multiple-taper spectral domain approach. Adv Geophys 41: 1–131

Mann ME, Park J, Bradley RS (1995a) Global interdecadal and century-scale climate oscillations during the past five centuries. Nature 378: 266–270

Mann ME, Bradley RS, Hughes MK (1998) Global-scale temperature patterns and climate forcing over the past six centuries. Nature 392: 779–787

Mann ME, Bradley RS, Hughes MK (1999) Northern Hemisphere temperatures during the past millennium: inferences, uncertainties, and limitations. Geophys Res Lett 26: 759–762

Mann ME, Bradley RS, Hughes MK (2000a) Long-term variability in the El Nino Southern Oscillation and associated teleconnections. In: Diaz HF, Markgraf V (eds) El Nino and the Southern Oscillation: multiscale variability and its impacts on natural ecosystems and society, Cambridge University Press, Cambridge, UK, pp 357–412

Mann ME, Gille E, Bradley RS, Hughes MK, Overpeck JT, Webb RS, Keimig FT (2000b) Annual temperature patterns in past centuries: an interactive presentation. Earth Interactions 4(4): 1–29

Marshall S, Oglesby RJ, Larson J, Saltzman B (1994) Comparison of GCM sensitivity to changes in $CO_2$ and solar luminosity. Geophys Res Lett 21(23): 2487–2490

Marshall S, Mann ME, Oglesby R, Saltzman B (1995) A comparison of the CCM1-simulated climates for pre-industrial and present-day $CO_2$ levels. Global Planet Change 10: 163–180

McHargue LR, Damon PE (1991) The global beryllium 10 cycle. Rev Geophys 29:141–158

Meehl GA, Washington WM (1996) El Niño-like climate change in a model with increased atmospheric $CO_2$ concentrations. Nature 382: 56–60

Miller AJ, Cayan DR, White WB (1998) A decadal change in the North Pacific thermocline and gyre-scale circulation. J Phys Oceanogr 27: 2023–2039

Minobe S (1997) A 50–70 year climatic oscillation over the North Pacific and North America, Geophys Res Lett 24: 683–686

Overpeck J, Hughen K, Hardy D, Bradley R, Case R, Douglas M, Finney B, Gajewski K, Jacoby G, Jennings A, Lamoureux S, Lasca A, MacDonald G, Moore J, Retelle M, Smith S, Wolfe A, Zielinski G (1997) Arctic environmental change of the last four centuries. Science 278: 1251–1256

Rind D, Lean J, Healy R (1999) Simulated time-dependent response to solar radiative forcing since 1600. J Geophys Res 104(D2): 1973–1990

Schlesinger ME, Ramankutty N (1994) An oscillation in the global climate system of period 65–70 years. Nature 367: 723–726

Stearns SD, David RA (1988) Signal processing algorithms. In: Oppenheim AV (ed) Prentice-Hall Signal Processing Series, Prentice-Hall, New Jersey, pp 349

Stocker TF, Schmittner A (1997) Influence of $CO_2$ emission rates on the stability of the thermohaline circulation. Nature 388: 862–865

Tett SFB, Stott PA, Allen MR, Ingram WJ, Mitchell JFB (1999) Causes of twentieth-century temperature change near the Earth's surface. Nature 399: 569–572

Timmerman A, Latif M, Voss R, Grotzner A (1998) Northern hemispheric interdecadal variability: a coupled air-sea mode. J Clim 11: 1906–1931

Tinsley BA (1988) The solar cycle and QBO influence on the latitude of storm tracks in the North Atlantic. Geophys Res Lett 15: 409–412

Tourre Y, Rajagopalan B, Kushnir Y (1999) Dominant patterns of climate variability in the Atlantic over the last 136 years. J Clim 12: 2285–2299

Trenberth KE (1990) Recent observed interdecadal climate changes in the Northern Hemisphere. Bull Am Meteorol Soc 71: 988–993

Trenberth KE, Hurrell JW (1994) Decadal atmospheric-ocean variations in the Pacific. Clim Dyn 9: 303–309

White WB, Cayan DR, Lean J (1998) Global upper ocean heat storage response to radiative forcing from changing solar irradiance and increasing greenhouse gas/aerosol concentrations. J Geophys Res 103 C: 21355–21366

White WB, Cayan DR (1998) Quasi-periodicity and global symmetries in interdecadal upper ocean temperature variability. J Geophys Res 103 C: 21335–21354.

Willson RC (1997) Total solar irradiance trend during solar cycles 21 and 22. Science 277: 1963–1965

Zhang Y, Wallace JM, Battisti DS (1997) ENSO-like interdecadal varibility: 1900–93. J Clim 10: 1004–1020